RMetS
Royal Meteorological Society

Soudano-Saharan depressions and their importance for precipitation and dust: a new perspective on a classical synoptic concept

K. Schepanski* and P. Knippertz
School of Earth and Environment, University of Leeds, UK
*Correspondence to: K. Schepanski, School of Earth and Environment, University of Leeds, Leeds, LS29JT, UK.
E-mail: K.Schepanski@leeds.ac.uk

According to a classical synoptic concept, Soudano-Saharan depressions (SSDs) are surface lows that track westward over tropical West Africa, curve anticyclonically across the Sahara and may then transform into eastward-moving Mediterranean cyclones. Occurrence frequency and track location undergo a marked seasonal cycle. Interactions between troughs in the upper-level westerlies and mid-level African easterly waves have been suggested as a mechanism for their formation. SSDs have been reported to be associated with dust-storms and precipitation over northern Africa.

This paper presents the first-ever systematic investigation of SSDs using re-analysis and satellite data. Depressions are identified and tracked objectively based on closed contours in 0000 UTC fields of 925 hPa geopotential height from the European Centre for Medium-Range Weather Forecasts ERA-Interim re-analysis (1989–2008). To classify as potential SSDs, tracks must: (i) start to the south of 20°N; (ii) intersect 15°–30°N, 10°W–30°E; (iii) cover a meridional distance of at least 10° latitude; and (iv) have a minimum lifetime of 24 hours.

Even with a relatively low threshold of 4 gpm, only 50 potential SSDs are found (annual average 2.5, monthly range 0–6). Lagrangian and Eulerian composite analyses reveal that the identified systems: (i) are mostly shallow lee troughs of the central Saharan and Atlas Mountains during the warm season without a well-defined cyclonic wind field; (ii) do not show the seasonal track variation described in the literature; (iii) mostly occur in association with high-pressure anomalies over the Mediterranean Sea; and (iv) are not associated with significant increases in dustiness and precipitation. These results strongly suggest that the disturbances described as SSDs do not manifest themselves as traceable low-level depressions, calling for a fundamental revision of the classical concept in the literature. Copyright © 2011 Royal Meteorological Society

Key Words: Africa; low-pressure system; lee trough; cyclone tracking; climatology

Received 23 October 2010; Revised 15 April 2011; Accepted 20 April 2011; Published online in Wiley Online Library 8 July 2011

Citation: Schepanski K, Knippertz P. 2011. Soudano-Saharan depressions and their importance for precipitation and dust: a new perspective on a classical synoptic concept. *Q. J. R. Meteorol. Soc.* **137**: 1431–1445. DOI:10.1002/qj.850

1. Introduction

Rainfall is the main limiting factor for bio-productivity and livelihood over semi-arid areas. Africa north of the Equator can be divided into an extratropical and a tropical rainfall regime (Nicholson, 1981), separated by the arid Sahara Desert. Along the Mediterranean coast, precipitation peaks during the winter season (November–March) and is closely

linked to extratropical disturbances such as midlatitude troughs, which usually track along the polar jet, but can occasionally migrate into the northern Sahara (Thorncroft and Flocas, 1997). In situations of strong northerly flow, blocking of low-level cold air by the Atlas Mountains can cause lee cyclogenesis, particularly during spring when the strong thermal contrast between the Mediterranean Sea and the continent enhances baroclinicity (e.g. Alpert and Ziv, 1989). To the south of the Sahara, over the Sahel and Soudan zones, the majority of the annual precipitation falls in connection with organised convection during the summer season (July–September), often related to African easterly waves (AEWs) (e.g. Buckle, 1996; Nicholson, 2000; Fink and Reiner, 2003). Interactions between tropical and extratropical disturbances, particularly during the transition seasons, can cause hybrid systems that have been termed Saharan depressions, Sahelio-Soudanian depressions or Soudano-Saharan depressions (SSDs) depending on their region of origin (Dubief and Queney, 1935; Dubief, 1947, 1963; Nicholson, 1981).

SSDs were first described by French and British meteorologists in the 1930s (Dubief and Queney, 1935), predominantly on the basis of the rare synoptic observations over the sparsely inhabited desert. SSDs are surface lows that cross the Sahara on an anticyclonic track from the Tropics to the subtropics, predominantly during spring and autumn, with little activity in summer (Nicholson, 1981; Buckle, 1996). According to various textbooks (Griffiths and Soliman, 1972; Warner, 2004) winter SSDs originate over the Atlantic south of 10°N, migrate northward and then turn sharply eastward towards the Sahara at about 15°N (Figure 1). During autumn, SSDs originate over the continent west of the Greenwich meridian and then turn north-eastward towards the Mediterranean Sea near 20°N. Spring tracks start further east and turn anticyclonically at about 15°N. SSDs have been associated with dust-storms, heavy showers and thunderstorms, particularly over elevated terrain, but also with fine and continuous dry-season precipitation known as Heug or Mango rains in the Sahel (Issar, 1995; Buckle, 1996; Leroux, 2001). In both cases, precipitation is related to the northward advection of humid air from the deep Tropics at the eastern side of the surface low (Issar, 1995). Due to evaporation in dry desert air, SSD-related precipitation decreases over the Sahara, where dust-storms are the main accompanying synoptic-scale weather events. To the best of our knowledge the exact nature of these dust-storms is not specified in the classical literature. Farther north, moist Mediterranean air can get incorporated into the SSD circulation and heavy rain can ensue (Nicholson and Flohn, 1980). The seasonality of rain in the Sahara has been linked to the occurrence of SSDs (Dubief and Queney, 1935; Nicholson, 2000) and even the increased aridity of the Sahara in recent centuries has been discussed in connection with a diminution of SSDs (Howell and Bourlière, 1963).

SSDs are assumed to develop through interactions of mid-level AEW disturbances with troughs in the upper-level westerlies over the subtropics (Flohn, 1975; Buckle, 1996). Their occurrence can be accompanied by the formation of a low-pressure corridor over northern Africa that causes a substantial break in the trade winds (Leroux, 2001). Pedgley (1972) described depressions embedded in such a pressure trough. Some of these systems migrate northward across the Sahara with little or no intensification, while others

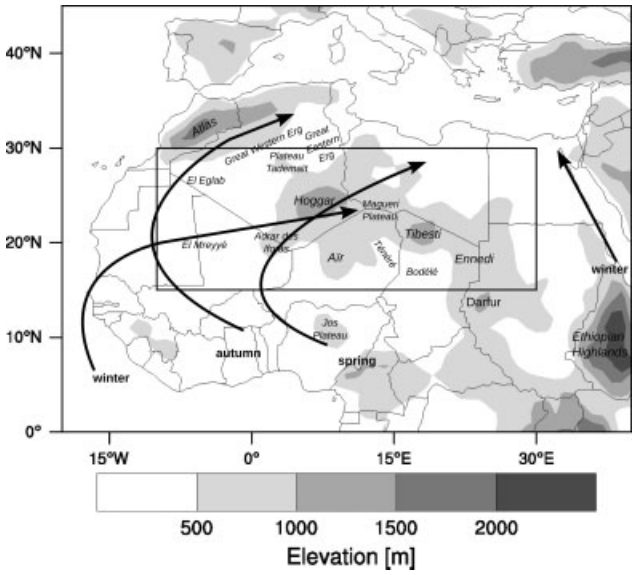

Figure 1. Overview of the area of interest. Shading represents ECMWF ERA-Interim model orography (m). Names of geographical features referred to in this paper are given in italics. The box surrounds the area through which depressions have to track to qualify as SSDs (section 3). Arrows represent seasonally varying SSD tracks as in Warner (2004).

intensify over northern Africa through positive vorticity advection at the eastern side of an upper-level trough in accordance with quasi-geostrophic reasoning. According to Buckle (1996), cyclonic storms are formed from easterly waves due to the influence of the upper-level trough. These storms migrate across the Sahara steered by a mid-level anticyclonic circulation.

During the summer season, large parts of West Africa are dominated by the Saharan heat low (SHL; Lavaysse *et al.*, 2009). The SHL shows variations in strength, position and extension on synoptic and intraseasonal time-scales (Chauvin *et al.*, 2010; Lavaysse *et al.*, 2010), sometimes resembling northward-tracking Saharan depressions. Enhanced southerly flow to the east of SHL disturbances transports moist, monsoonal air from the Tropics into the Sahara leading to a higher potential for convection, while drier air and high convective inhibition occurs to the west (Sultan and Janicot, 2003). The Saharan orography plays a role in the formation and variations of the SHL through lee-trough effects when the northeasterly trade winds encounter the Atlas–Hoggar Mountain ridge (Sultan and Janicot, 2003; Drobinski *et al.*, 2005).

During high-pressure situations over the central Mediterranean Sea a temperature anomaly called 'cold air surge' by Vizy and Cook (2009) may develop and reach from the Mediterranean coast into the Sahara. It is understood to be responsible for transport of moist air from the Mediterranean Sea into the Sahara–Sahel region, where it can influence local rainfall. Linked to the cold surges described by Vizy and Cook (2009), Chauvin *et al.* (2010) characterise the intraseasonal variability of the SHL with two different phases ('west' phase and 'east' phase) with a time-scale of about 14 days. The west phase is characterised by a central Mediterranean high and strong winds over Libya causing a cold surge. The east phase is characterised by a northward extension of the SHL and a strong Azores high over the east Atlantic.

The relationship between the classical concept of SSDs, SHL variations, cold surges and the Saharan orography has

never been systematically investigated. The main aim of this study is therefore to use the possibilities offered by modern re-analysis and satellite data together with an objective identification algorithm to reappraise the SSD concept and to place it into the context of the existing literature. In particular this study will verify: (i) the proposed seasonal changes of SSD tracks; (ii) the role of tropical–extratropical interactions and AEWs for SSD initiation and propagation; (iii) the role of Saharan orography; and (iv) the relation of SSDs to unsettled weather, i.e. precipitation over arid areas and dust-storms. To the best of our knowledge this is the first-ever systematic investigation of SSDs.

The remainder of the paper is structured as follows: section 2 describes the data employed, followed by an explanation of the identification and tracking algorithm. In section 3 a selected SSD case is discussed, to better illustrate results in sections 4 and 5 on statistical characteristics of SSDs and the larger-scale atmospheric conditions they are embedded in, respectively. Finally, section 6 discusses the findings of this study in the light of the existing literature, while section 7 contains some concluding remarks.

2. Data and methods

2.1. Re-analysis data and surface observations

Large-scale geopotential-height, wind and temperature information are taken from the ERA-Interim re-analysis dataset provided by the European Centre for Medium-range Weather Forecasts (ECMWF) (Berrisford *et al.*, 2009). The data were interpolated from the original spectral resolution of T255 to a $1^\circ \times 1^\circ$ horizontal grid and are available every six hours for the 20-year period 1989–2008. In addition, three-hourly synoptic station reports (SYNOPs) of wind, temperature, humidity, pressure, visibility, precipitation, clouds as well as present and past weather from several northern African weather stations are used. These are taken from the MIDAS archive in the Global Weather Observation dataset provided by the British Atmospheric Data Centre funded by the UK Natural Environment Research Council (http://badc.nerc.ac.uk).

2.2. Satellite data

To investigate the relation of SSDs with rainfall, the three-hourly Tropical Rainfall Measuring Mission (TRMM) precipitation product 3B42 in $0.25^\circ \times 0.25^\circ$ horizontal resolution is used. It is based on a combination of measurements at microwave and infrared (IR) wavelengths from various satellites with the space-borne TRMM precipitation radar to achieve full coverage in space and time after calibration on a monthly basis with surface gauge data (Huffman *et al.*, 2007). The 3B42 product is available from 1998 to the delayed present. As a proxy for high clouds, outgoing long-wave radiation (OLR) estimates based on measurements in thermal IR channels from National Oceanic and Atmospheric Administration (NOAA) low Earth-orbiting satellites are used (Liebmann and Smith, 1996). These are available as daily global fields in $2.5^\circ \times 2.5^\circ$ horizontal resolution since 1974.

To detect dust signals in association with SSDs, the semi-quantitative aerosol index (AI) from the polar-orbiting Total Ozone Mapping Spectrometer (TOMS) and the qualitative dust index from the geostationary Meteosat Second Generation (MSG) satellites are used. The former is based on the spectral contrast between the ultraviolet (UV) wavelengths of 340 and 380 nm caused by back-scattering effects from UV-absorbing aerosols like dust and soot particles (Herman *et al.*, 1997). The AI product is available on a daily basis at a horizontal resolution of $1.0^\circ \times 1.25^\circ$. The TOMS instrument was flying on Nimbus-7 from 1978 to 1993 and on Earth Probe from 1996 to 2005. Both satellites were flying on a Sun-synchronous orbit passing over the Equator at local noon. The MSG dust index is an RGB (red, green and blue) false-colour depiction using brightness temperatures (BT) from three thermal IR channels measured by SEVIRI (Spinning Enhanced Visible and IR Imager). Red is given by the BT difference between 12.0 μm and 10.8 μm, green by the difference between 10.8 μm and 8.7 μm and blue by the BT at 10.8 μm (Schepanski *et al.*, 2007). The dust index is available every 15 minutes and has been used extensively for studies on mineral dust (e.g. Schepanski *et al.*, 2007, 2009; Knippertz *et al.*, 2009; Knippertz and Todd, 2010).

2.3. Identification and tracking

Identification and tracking of potential SSDs are done with a modified version of an algorithm originally developed by Wernli and Schwierz (2006) for extratropical cyclones, applied to the domain 10°S–45°N and 40°W–60°E. In contrast to Wernli and Schwierz (2006), 925 hPa geopotential height fields are used instead of mean-sea-level pressure to account for the elevated terrain over most of northern Africa (Figure 1). In addition, several thresholds used for the identification and tracking were adapted to low-latitude conditions. The identification procedure consists of four main steps:

1. Identification of local minima relative to the eight neighbouring grid cells (1° grid spacing).
2. Determination of the outermost closed contour around each minimum. For this study a relatively small value of 4 gpm was chosen, which corresponds to a pressure interval of ∼0.5 hPa (Wernli and Schwierz (2006) use 2 hPa for comparison). Smaller and larger contour intervals were tested extensively, but 4 gpm gave the most satisfactory results relative to subjective eye analyses.
3. Grid points within (outside of) the outermost closed contour are masked by '1' ('0').
4. Geographic position of the centre, minimum geopotential height, value of the outermost closed contour and size of the depression are registered.

In Wernli and Schwierz (2006), the tracking of disturbances is done by comparing the position of an identified minimum with a first guess computed from a reduced linear continuation of the track during the previous 24-hour time interval allowing a maximum deviation of 1000 km. This procedure allows determining genesis, lysis (weakening), track and lifetime of each system. Such an approach is difficult to apply to northern Africa due to the large diurnal variations in pressure and geopotential height caused by atmospheric tides and heat-low effects, which affect the identification of individual minima and their linkage into tracks using 6-hourly data. In principle, one can circumvent this problem by either using 24-hour time steps or by

removing the average diurnal cycle from the 6-hourly data. After some testing against subjective identification and tracking, the authors decided to use the former approach applied to 0000 UTC fields and with a maximum distance between two centres of 1000 km, which correspond to a daily average propagation velocity of 11.6 m s^{-1}. Midnight was chosen to keep the influence of sensible heating/cooling to a minimum. Such an algorithm would not work for fast-moving cyclones in midlatitude storm tracks, but gives satisfactory results for low latitudes as demonstrated in section 3.

To filter systems consistent with typical SSD characteristics as described in the literature, the following additional criteria were applied:

- Track begins to the south of 20°N.
- Track intersects main area of interest 15°N–30°N and 10°W–30°E (box in Figure 1). In this way, Atlantic cyclones, midlatitude disturbances, depressions developing over the Arabian Peninsula and tropical disturbances over central Africa are excluded.
- Track covers at least a latitudinal distance of 10°. This excludes stationary systems, which are likely to be related to local diabatic effects, and AEWs which are tracking westward, but do not curve anticyclonically across the Sahara as described for SSDs in the literature (see section 1).
- Track is mostly northward with a starting point to the south of the ending point. This excludes midlatitude disturbances penetrating into the Sahara and again most westward-tracking AEW disturbances.

3. A case-study example: 6–14 June 2006

To illustrate results from the objective identification and tracking, an example of an SSD during June 2006 will be discussed in this section. The track and geopotential height minima of the SSD are shown in Figure 2. The system forms to the southwest of the Tibesti Mountains on 6 June and initially tracks westward across Niger and Mali. At any one time the system lies in the vicinity of mountains. On 7 June the system is located south of the Aïr Mountains, on the leeward side with respect to the northerly harmattan flow. On 8 June the SSD lies to the east of the Adra des Iforas. The system continues in a westward direction and then turns northward around the western side of the Adrar des Iforas Mountains on 9 June. It crosses the Sahara near 5°W on 10 and 11 June to reach the southern side of the High Atlas Mountains, where it remains on 12 and 13 June. By 14 June the system has crossed the Atlas chain to reach the Mediterranean coast of northeastern Morocco. The minimum geopotential height varies between 735 and 761 gpm during this 9-day period with no clear trend. The southern part of this track is also discussed by Couvreux *et al.* (2010) in the context of synoptic-scale variations of the monsoon flow. It should be noted that, according to the literature, June is outside the period of strongest SSD activity (see Introduction). The track discussed here, however, has some resemblance to what has been described as a typical autumn track (Figure 1).

Figures 3 and 4 show the evolution of 925 hPa geopotential height, precipitation, clouds and dustiness during this period. On 6 June 2006 a pronounced high-pressure system is located over the central Mediterranean Sea creating a strong meridional gradient in geopotential height

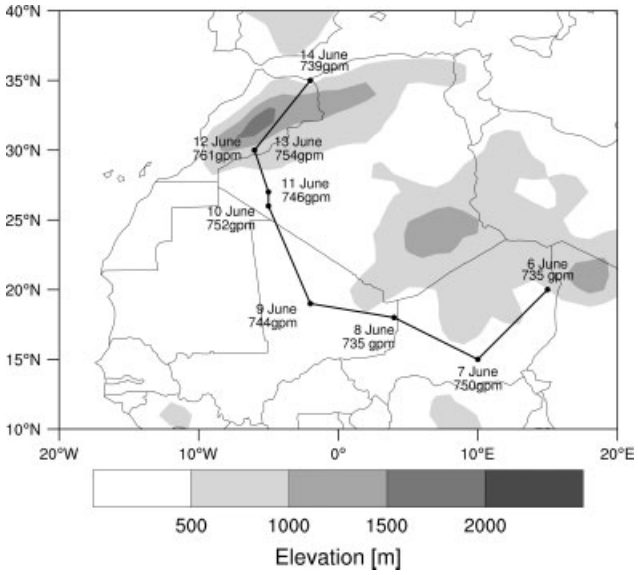

Figure 2. An example case-study of an SSD during 6–14 June 2006. The thick solid line shows the SSD track and filled circles the positions of the centre as identified by the algorithm described in section 2. Day of June 2006 and minimum geopotential height are given. Shading represents ECMWF ERA-Interim model orography (m) as in Figure 1.

towards the elongated SHL stretching from the Arabian Peninsula across West Africa (Figure 3(a)). Two individual and separately identified minima with closed contours are evident over the Sahel: a rather small one over the Grand Erg de Bilma close to the border of Niger and Chad (minimum at 19°N 15°E, 736 gpm), and a more substantial one over central Chad (15°N 20°E, 734 gpm). Both disturbances track westward and merge until 7 June at 15°N 10°E (Figure 3(c)). Due to the shorter distance, the automatic tracking routine identifies the smaller disturbance as the initiation location (see Figure 2). This depression develops from a lee trough associated with north-easterly winds on the western side of the Tibesti, as indicated by Froude numbers <1 in the region around 20°N 16°E on 6 June (not shown). The Froude number F_r is the non-dimensional ratio between the wind speed v and the Brunt–Väisälä frequency N of the oncoming flow and the maximum height of the mountain h_m, $F_r = v/h_m N$. For $F_r < 1$, part of the low-level air is blocked by the obstacle, favouring the development of a lee trough. MSG satellite images indicate a convective disturbance further to the southeast over the region of the Darfur Mountains, mid-level clouds over the region west of the Tibesti and a dust front developing on the mountain ridge between the Hoggar Massif and Tibesti, potentially caused by strong harmattan winds forced by the meridional pressure gradient (Figure 3(b)). Precipitation is falling associated with the convective disturbance over the Darfur Mountains region (Figure 3(a)).

On 7 June the SSD is located over central Niger in the lee of the Aïr Mountains (Figure 3(c)). The associated low-pressure zone over the southern central Sahara and therefore the meridional pressure gradient have weakened. MSG images and SYNOP reports indicate dust in the vicinity of the SSD over the Aïr, Adra des Iforas and Hoggar Mountains, the Magueri Plateau between the Hoggar and the Tibesti Mountains, and the Ténéré (Figure 3(d)). Looking at 15-minute resolution MSG images, dust uplift appears to be related to harmattan winds and so-called haboobs over

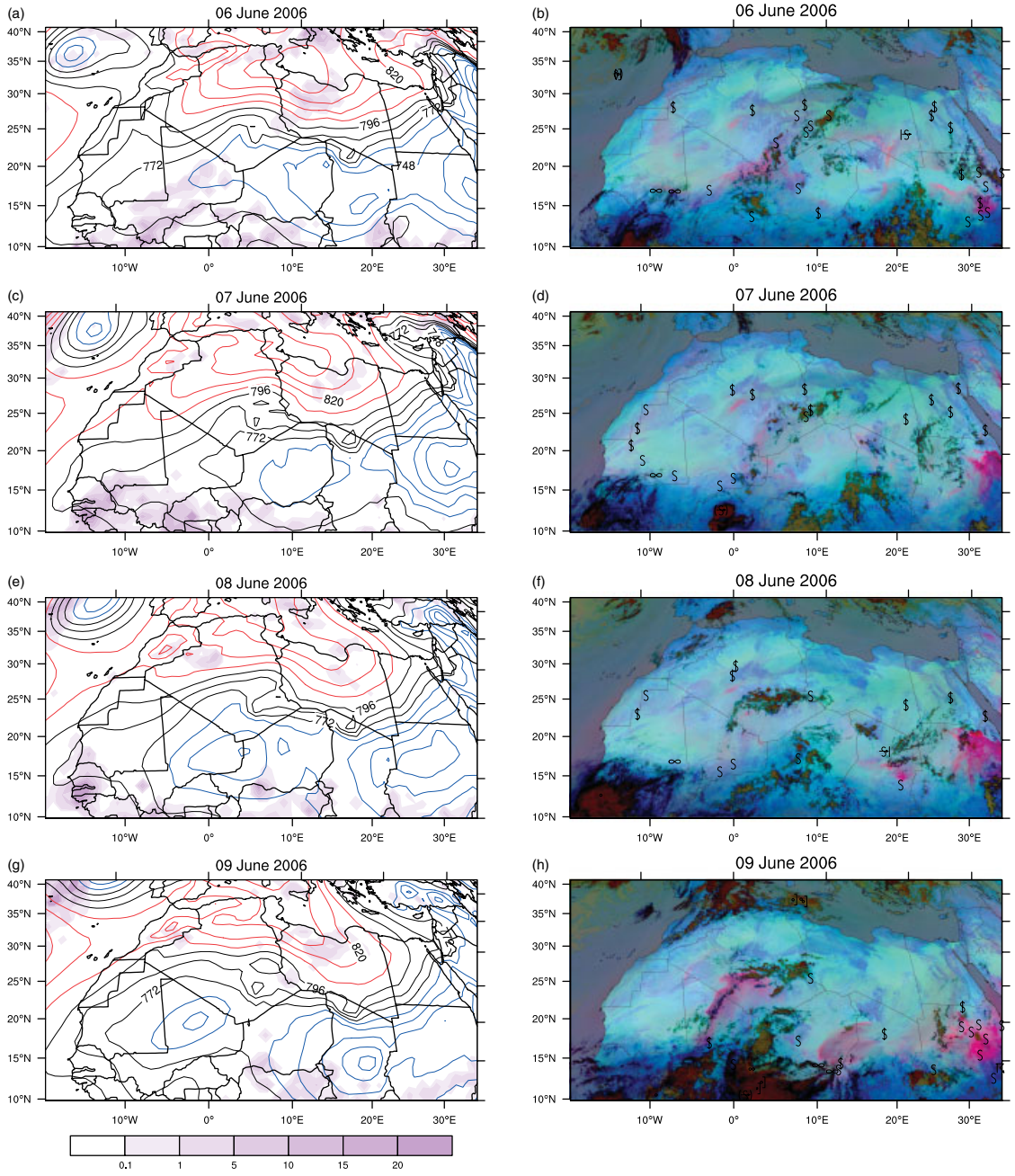

Figure 3. Time evolution of the SSD example case during 6–9 June 2006. Daily 0000 UTC ECMWF ERA-Interim 925 hPa geopotential height fields (gpm) with daily precipitation (mm d^{-1}) from TRMM 3B42 product (shaded colour; left column), and daily 1200 UTC MSG IR dust images and SYNOP reports (right column, Copyright © EUMETSAT 2006). Geopotential height: Isohypses are given by contour lines at 12 gpm intervals. Blue 700–760 gpm, black 772–796 gpm, and red 808–868 gpm. MSG images: Pinkish colour indicates airborne dust, dark-reddish colour deep convective clouds, green colour thin, mid-level clouds, and brownish colour thick mid-level clouds. Synoptic observations of present weather are given by black symbols according to World Meteorological Organisation's present-weather code. For the sake of clarity only weather symbols related to dust/sand, precipitation and thunderstorms are shown.

the central Saharan mountains during the night. The latter are dust-storms at the leading edge of cold pools caused by the evaporation of precipitation from deep convection (e.g. Knippertz and Todd, 2010).

On 8 June the high-pressure zone has retreated somewhat to the western Mediterranean Sea (Figure 3(e)). The centre of the SSD is now located on the southwestern side of the Hoggar Massif. Froude numbers <1 indicate favourable conditions for a lee trough. This is the first time that wind vectors at 925 hPa indicate a clear cyclonic circulation around the centre of the depression (not shown). The MSG image highlights a cluster of convective clouds over the

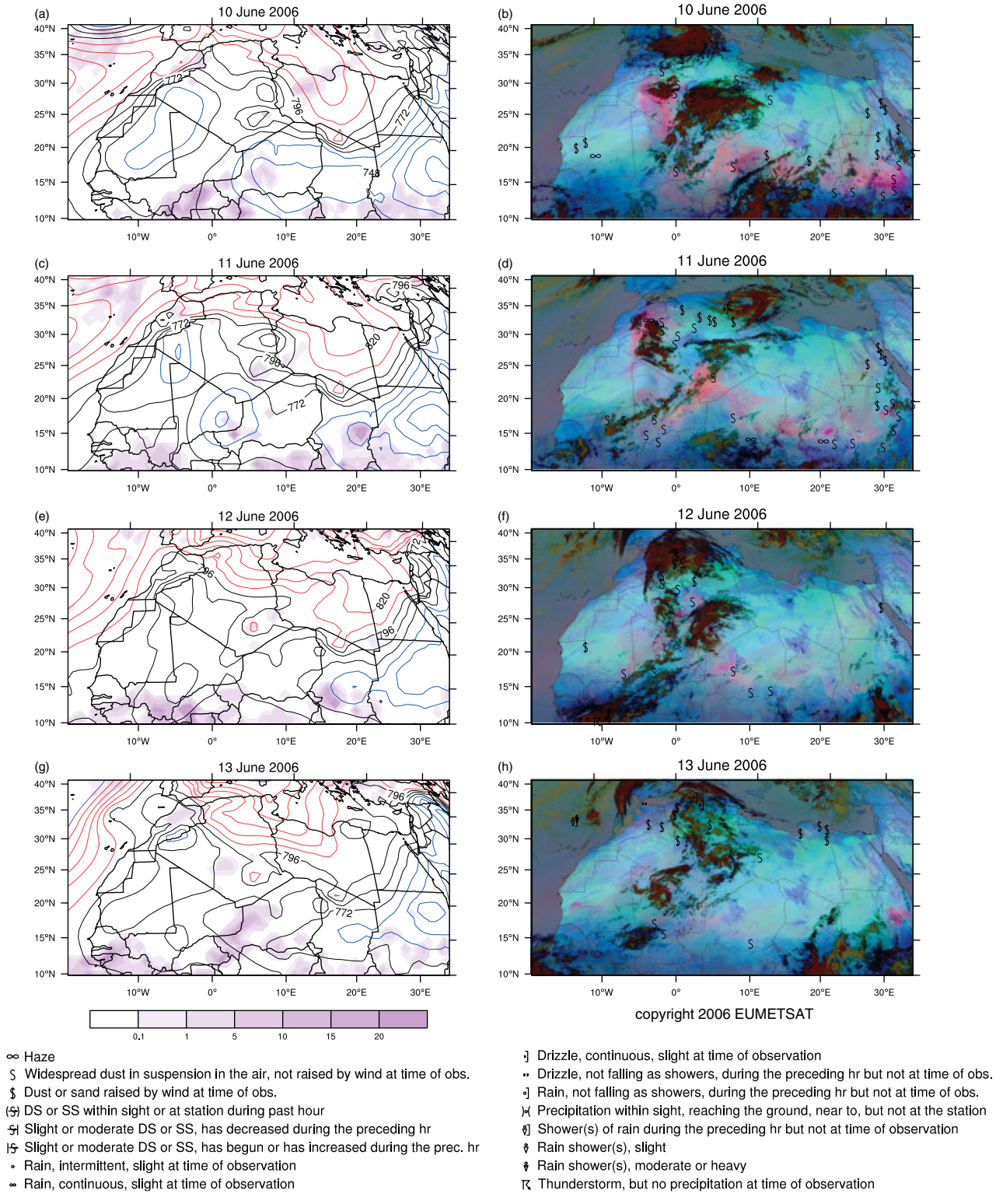

Figure 4. As Figure 3 but for 10–13 June 2006 (right column images Copyright © EUMETSAT 2006).

Hoggar Massif causing dust-storms (Figure 3(f)) but no precipitation reaching the ground (Figure 3(e)).

Until 9 June the ridge continues to retreat northwestwards over the Mediterranean, while the SSD centre migrates westwards into central Mali (Figure 3(g)). A mesoscale dust front, highlighted by the MSG dust image and SYNOP reports, extends south from the Hoggar Massif crossing Mali and the SSD centre (Figure 3(h)). A detailed inspection of MSG images reveals that the majority of this dust is connected to haboobs and consequently advected northwestwards, and not directly to the larger-scale cyclonic circulation associated with the SSD itself (not shown). Deep convection is most active during the evening and night on 8 to 9 June, fostered by advection of moist monsoonal air from the south on the eastern side of the SSD. Early indications of moist convection over the Hoggar Massif can be seen in Figure 3(f); remnants of the clouds are still evident the next day (Figure 3(h)). According to the TRMM product no precipitation reached the ground over this area.

On 10 June the low-pressure zone shifts northward and the disturbance is now centred over the El Eglab Plateau in western Algeria (Figure 4(a)). The high-pressure ridge over the Mediterranean Sea still reaches deep into the Sahara over Libya. Deep convection develops over the Great Western Erg south of the High Atlas Mountains and over the Hoggar Massif causing dust-storms (Figure 4(b)). A large dust front generated by cold outflows of clouds over the Aïr and Hoggar Massif during the previous night is observed to track in a northwesterly direction. According to the TRMM rainfall product, precipitation reached the ground over the Atlas region and the Hoggar Massif. Triggered by the penetration of a weak upper-level trough into northwestern Africa (not shown), pressure falls on the Saharan side of the Atlas Mountains.

Between 10 and 11 June the centre of the SSD shifts northward by about 1° across western Algeria and continues to deepen (Figure 4(c)). Deep convection associated with some rainfall develops close to the Atlas Mountains with more rain falling over the Hoggar Massif (Figure 4(c) and (d)). Linked again to cold outflows generated by deep convection, dust-storms develop, especially over the Great Western Erg and the Atlas Mountains area (Figure 4(d)). With the upper-level disturbance slowly decaying over western Algeria (not shown), the SSD remains almost stationary on 12 and 13 June (Figure 4(e) and (g)). Convection is still deep and causes widespread dust-storms, especially over the Great Western Erg, the Atlas and Hoggar Massif region as indicated by the MSG dust image and reported by weather stations (Figure 4(f) and (h)). Despite the widespread convective activity, rather little precipitation reached the ground according to the TRMM rainfall product. Finally the SSD crosses the Atlas Mountains on 14 June (Figure 2).

In order to test a possible relationship of this SSD to cold surges, Figure 5 shows zonal mean temperature anomalies at 850 hPa for 10–30°E, an area where air mass transport from the Mediterranean Sea towards the desert is not disturbed by zonally orientated mountain ridges. Two cold air surges are evident: The first occurs from 8 to 11 June 2006 and extends southward towards about 20°N. During this period the high-pressure ridge over the Mediterranean Sea stretches into Libya, and the SSD tracks across Mali into western Algeria (Figures 3 and 4). The second surge is evident from 13 June onwards and is most likely not directly related to the SSD. The days leading up to the first cold surge (6–9 June 2006) resemble the SHL west phase of Chauvin *et al.* (2010), while the decay from 10 to 12 June 2006 fit the east phase (compare Fig. 6 in Chauvin *et al.*with Figures 3 and 4). These results suggest that the early stages of the SSD development is closely related to a blocking of the relatively cool and moist northeasterly flow from the Mediterranean over Libya and east Algeria by the Aïr–Hoggar–Tibesti mountain chain. This mechanism has not been described in the literature and is a genuine finding of this study.

In order to investigate the role of AEWs for the westerly leg of the SSD track, a Hovmüller diagram for 700 hPa meridional wind at 15°N is shown in Figure 6. During 6–14 June 2006 two AEWs develop and propagate westwards. Southerly winds on the eastern side of the wave trough transport moist monsoonal air northwards, while the northerlies on the western side bring dry desert air southwards. Between 6 and 8 June a weak AEW propagates from the Greenwich meridian to the Atlantic with moist convection to the east of the wave axis (e.g. Figure 3(b)). This system is too far west to interact with the SSD. A second wave develops on 8 June with its trough axis located at about 10°E and is also accompanied by deep convection (Figure 3(f)). This AEW migrates westwards and reaches the Atlantic on 11 June. Assuming a typical baroclinic tilt with height, the SSD under study is most likely related to the low-level signal of this AEW between 8 and 10 June as suggested in the literature.

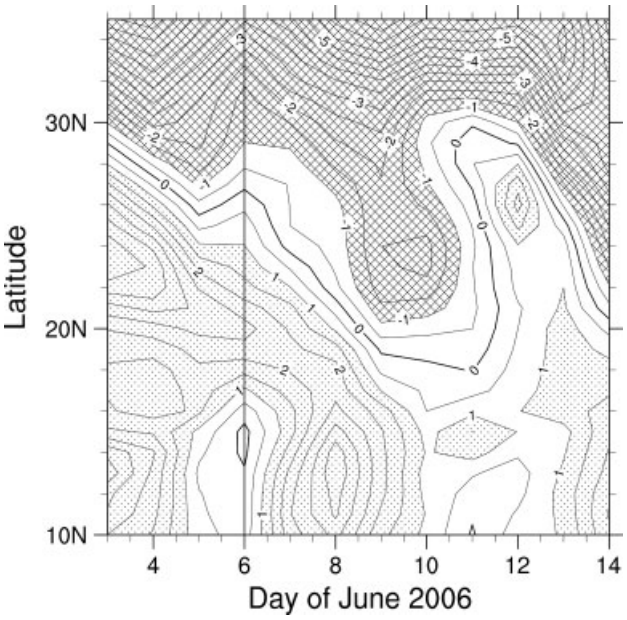

Figure 5. Relation of example SSD to cold surges. Hovmüller diagram of 850 hPa temperature (K) anomaly with respect to a long-term mean, zonally averaged over 10°E to 30°E. The period shown is 3–14 June 2006. The track of the SSD starts at day 6 (marked by a black vertical line) and ends at day 14. Negative values (striped area) indicate the transport of cooler air from the Mediterranean Sea towards the Sahara by northerly winds related to a high-pressure zone over the Mediterranean Sea.

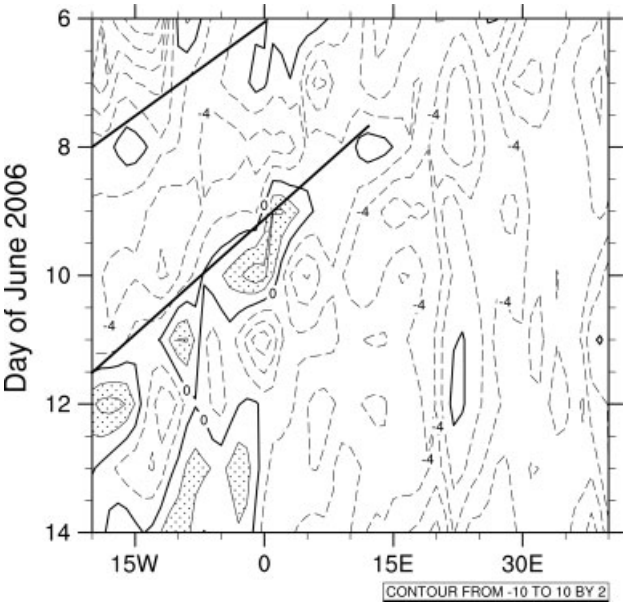

Figure 6. Relation of example SSD to AEWs. Hovmüller diagram of the meridional wind (m s^{-1}) at 700 hPa along 15°N for 6–14 June 2006. Negative, i.e. northerly, winds are given by dashed contours, southerly winds by solid contours. Westward propagating areas of negative meridional wind indicate westward propagating AEWs (marked by black lines).

As discussed above, a number of precipitation events occur across the Sahara linked to convective storms to the east of the SSD during the westward and northward part of the track, but some of these are quite far from the SSD centre. Dust-storms are frequent during the Saharan part of the track and are mainly caused by haboobs or by strong harmattan winds in the early stages. Cyclonic winds directly associated with the pressure disturbance of the SSD appear to play a smaller role.

4. Climatological analysis

Applying the algorithm described in section 3 to the 20 years of ERA-Interim data from 1989 to 2008 yields 50 identified systems (2.5 per year on average). This number appears relatively small in the light of the literature results, particularly given the fairly relaxed criteria of a contour interval of only 4 gpm and a minimum lifetime of 1 day. In the following, a detailed climatological analysis for these 50 systems will be presented to investigate their seasonal and interannual behaviour as well as their mean characteristics.

Annual numbers of identified systems vary strongly between zero in 1989 and 1991 and 6 in 2000 (Figure 7(a)). Total numbers of systems per month over the 20-year period reveal no activity at all for December to February and highest occurrences for May (10), April (8) and June (7) (Figure 7(b)). July stands out as the month with the smallest number of systems during the generally more active summer half of the year, April to September. Most-active single months are April 1999 and May 2000 with 3 identified systems per month (not shown). These results are not fully consistent with the literature, which claims maxima in spring and autumn and little activity in summer (Nicholson, 1981; Buckle, 1996).

In order to better understand these variations, correlations to the North Atlantic Oscillation index (NAO; Barnston and Livezey, 1987) are calculated, which represents the variability of the dominant large-scale pressure pattern over the North Atlantic, namely of the Icelandic low and the Azores high. The position and strength of each centre determine the large-scale wind regime, precipitation and temperature over the North Atlantic, Europe and North Africa (e.g. Hurrell, 1995; Jones *et al.*, 1997). During a positive phase of the NAO, the trade winds are strengthened and strong harmattan surges can occur. A correlation between an NAO index and the number of SSDs per month does not show evidence for a significance relation (correlation coefficient: −0.13). This could to some extent be related to an NAO activity maximum in winter when no SSDs are observed.

Figure 7(c) shows the median and range of SSD lifetime for each month. The median varies between 4.5 days in November and 9 days in May. Some systems in May and August live more than two weeks. The minimum lifetime of 3 days is probably related to the selection criterion to cross at least 10 degrees of latitude (see section 2). Overall during the 20 years, most depressions live for 5–6 days. Track length is closely linked to lifetime, suggesting a rather narrow range of propagation velocities (Figure 7(d)). Measured along a great circle to account for the Earth's curvature, tracks range between 1400 km and 6500 km. May shows the highest median, August the longest track. Tracks tend to be longer during spring than during autumn. The case discussed in section 3 shows above-average lifetime (9 vs. 8 days) and track length (4102.96 km vs. 2729.48 km).

By computing the frequency of how often a given grid cell is part of an identified depression, a horizontal distribution of track density can be generated (Figure 8). The main area of activity spans the entire African continent between about 10 and 20°N and then extends northward to the southern side of the Atlas chain between 10°W and 15°E. No activity is recorded for northeastern Africa including eastern Libya, Egypt and northern Sudan. A small confined maximum occurs over southern Spain suggesting that some systems manage to cross the Atlas as in the case-study in section 3. This general pattern is broadly consistent with the literature results as sketched in Figure 1. The identified systems have a prevalence to form in or pass through regions to the southwest or west of elevated terrain in the southern part of the active region (see stippled areas in Figure 8). Track densities of up to 7–8% are found close to the Hoggar, Adrar des Iforas and Aïr Mountains, while some weaker maxima occur to the southwest of the Tibesti and to the west of the Darfur and northern Ethiopian Highlands. Given that these areas are subject to the low-level northeasterly harmattan flow for most of the year, the most active regions are located downwind of the mountains, strongly suggesting that lee troughing plays an important role in initiating these disturbances as discussed in the case-study in section 3. It should be stressed that lee troughs in the vicinity of the Saharan mountains are not evident in climatological means (not shown), indicating the transient nature of the disturbances. Two other localised maxima stand out in Figure 8(a): one over western Algeria to the southeast of the High Atlas Mountains reaching values of more than 8%, and a very prominent maximum on the northern side of the Hoggar close to the Algerian–Libyan border with values of more than 12%. The former is a well-known region for lee cyclogenesis (e.g. Egger *et al.*, 1995; Horvath *et al.*, 2006) in situations of cool northwesterly flow impinging on the High Atlas. For the area to the north of the Hoggar, lee effects do not appear a likely explanation, as the flow is predominantly easterly or northeasterly in this region. Instead the area is characterised by plateaus and ergs, which foster the development of localised heat lows. This effect could cause SSDs to propagate into this area.

Splitting track densities into spring, summer and autumn (Figure 8(b)–(d)) reveals little geographical variations, which casts some doubt on the concept of seasonally varying tracks described in the literature (see Fig. 1 in Griffiths and Soliman, 1972). The prevalence for southern and western parts of the Saharan mountains and the southeastern side of the Atlas is evident for all three seasons, although areas of maximum density vary. During the most active spring (Figure 8(b)), tracks cover the largest area, with several conspicuous local maxima. Track densities of more than 4% are evident on the southwestern side of the Ennedi and Darfur Mountains, and the Adrar des Iforas Massif. Less pronounced maxima (3–4%) occur to the southwest of the Tibesti and the Magueni Plateau. Highest densities during spring are observed on the northern side of the Hoggar Massif (up to 7%). During summer (Figure 8(c)), tracks cluster more in the western part of the region, the area of the climatological SHL (Lavaysse *et al.*, 2009). High track densities are observed along the southeastern part of the Atlas Mountains (up to 4%) and over a corridor around the Aïr, Adrar des Iforas and Hoggar Massif. Three maxima stand out: one to the southeast of the Aïr (4%), one to the west of the Hoggar (5%), and one to the north of the Hoggar

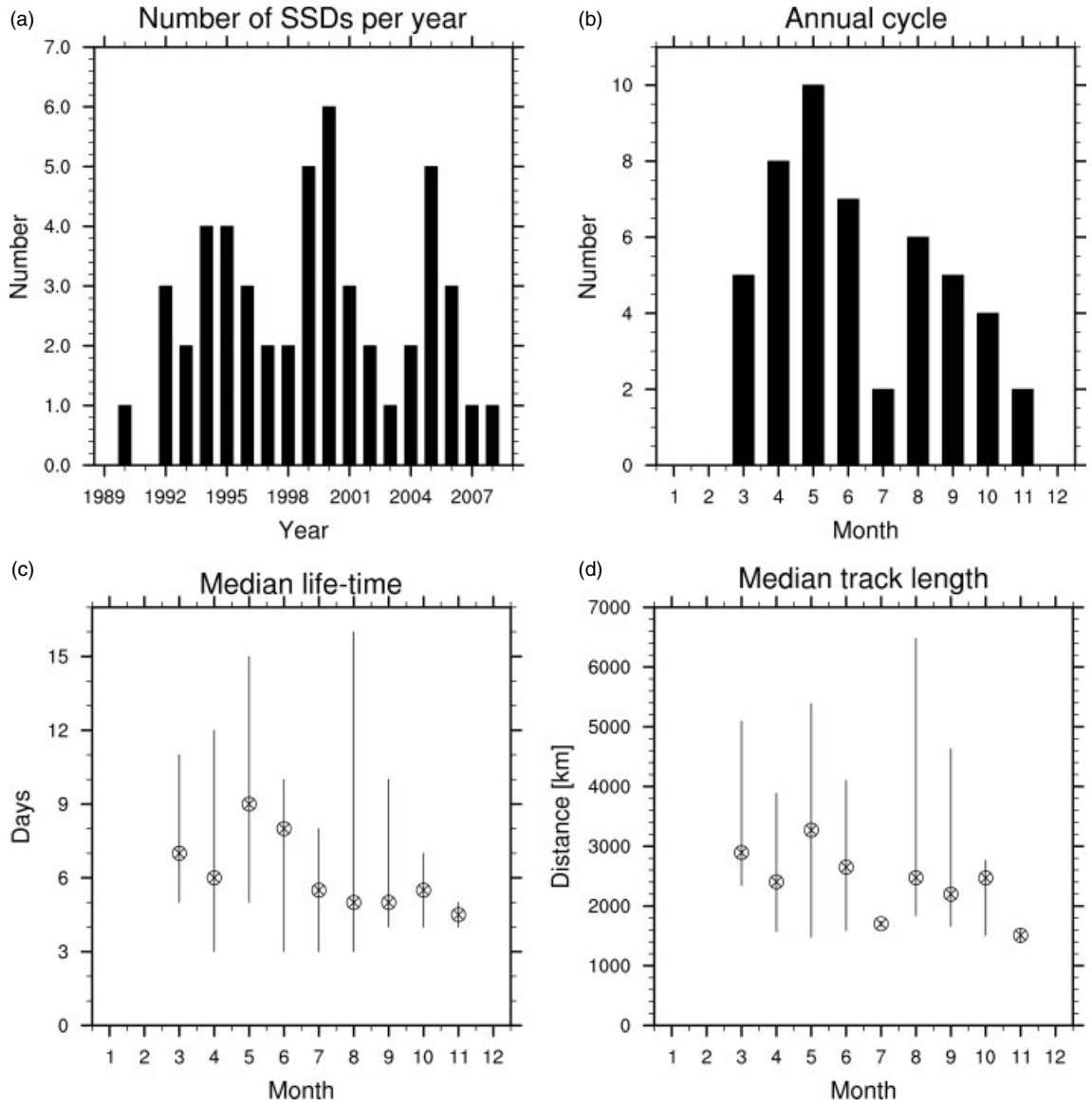

Figure 7. SSD climatology for the 20-year period 1989–2008. (a) Number distribution of identified systems per year adding up to 50 in total, and (b) total SSD numbers per month. Median (crossed circle), and range (whiskers) of (c) lifetime and (d) track length per month.

(up to 7%). Compared to spring and autumn, higher track densities are observed over eastern Mauritania and western Mali, especially over the El Mreyyé dune field. Heat-low effects over the Iberian Peninsula support a northward tracking of depressions across the Atlas with track densities of up to 4%. SSD activity is lower in autumn (Figure 8(d)). Two areas of higher track densities of 3% stand out, one to the southwest of the Aïr and one to the southeast of the Atlas.

Spatial distributions of SSD genesis (Figure 9(a)) show that during all seasons a significant portion of SSDs develop in the vicinity of mountains, especially on the southern to western side of the Saharan mountains, the leeward side with respect to the harmattan flow. Consistent with an anticyclonic turning of SSD tracks, pronounced regions for SSD lysis are located on the northern side of the Saharan mountains in all seasons (Figure 9(b)). Spring SSDs tend to transform into Mediterranean cyclones with lysis locations over northern Libya and Egypt. This is consistent with the peak of the Atlas lee cyclogenesis season described in the literature (Alpert and Ziv, 1989).

Finally, in order to test the influence of AEWs on SSDs, Hovmüller diagrams of 700 hPa meridional wind at 15°N for all identified systems were inspected. Out of the 50 SSDs less than 15 coincide with AEWs and may have interacted with them as in the case described in section 3. This is again in some contrast to the mechanisms proposed in the literature (see Introduction).

5. Composite analysis

To identify atmospheric conditions characteristic of the identified systems and the environments they form in, composite plots following Eulerian and Lagrangian approaches are computed. For the former, temporal mean fields for all time periods with at least one identified system are computed for the entire geographical domain 10°S–45°N and 40°W–60°E. This allows characterising the large-scale environment and relationships to geographically fixed features, but may smear out the signal of the propagating disturbance itself. Lagrangian composites are constructed in a similar way, but relative in space to the centre of an

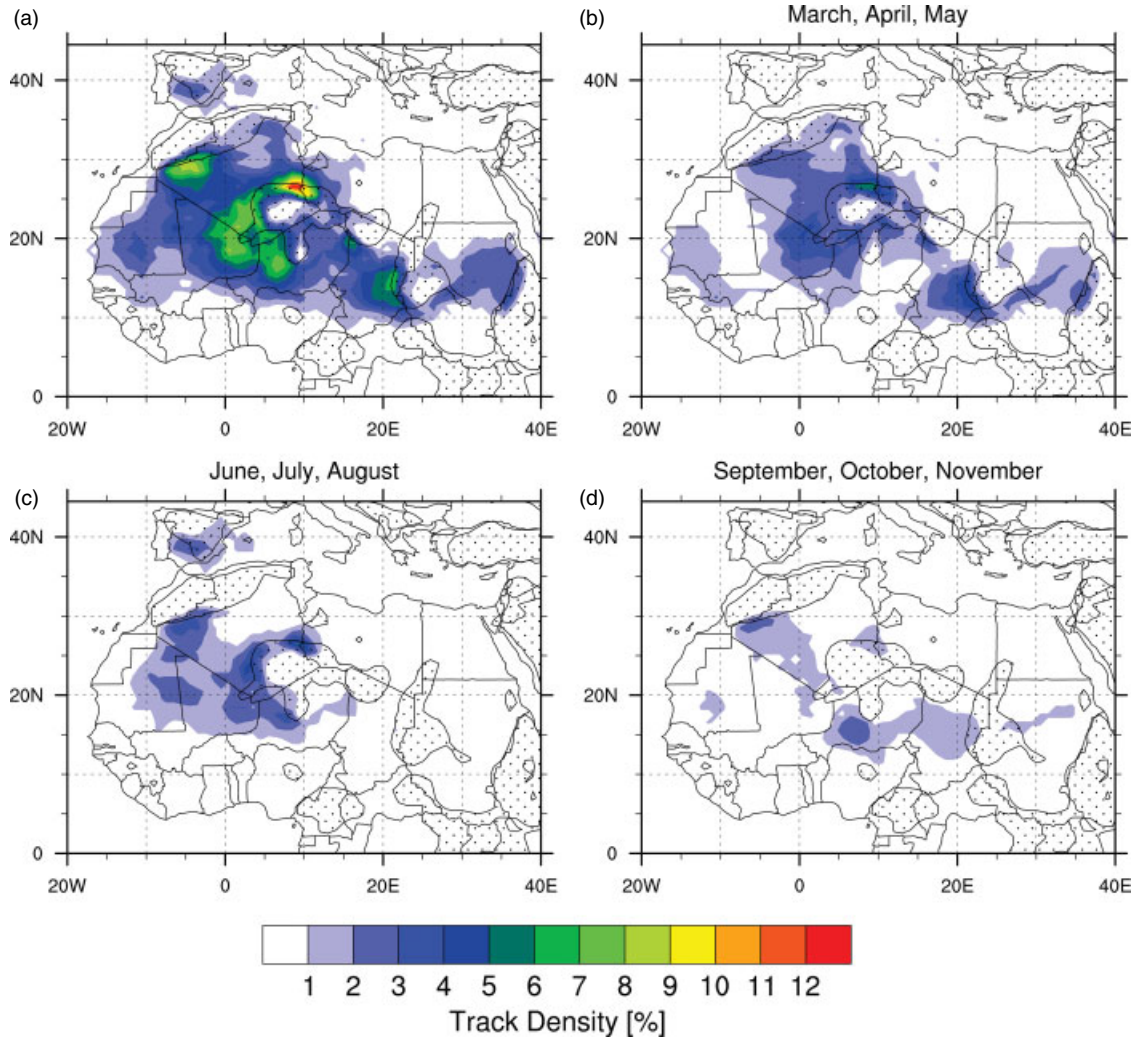

Figure 8. Horizontal distribution of SSD track density defined as the frequency (%) of grid cells to be identified as part of an SSD. Shown are (a) yearly, (b) spring, (c) summer and (d) autumn. No SSDs are identified for winter within this study. Dotted areas indicate orography higher than 600 m.

identified system over a domain of ±5 degrees in each direction. This approach allows representing time-mean features linked directly to the depression itself. Both composites will, of course, have strongest contributions from periods with most SSD occurrence, i.e. spring/early summer and autumn (Figure 7(b)). Assessing the statistical significance of composites is not trivial. Here some tests were carried out on the basis of Monte Carlo calculation following ideas discussed in Moore *et al.* (2008):

(1) For each of the 50 SSDs, 300 days were chosen out of a ±10-day period around the SSD start date (or end date) for each year (1989–2008) except for the SSD period itself. This leads to 300 random 50-member composites with the same seasonal distribution as the SSD composite (Figure 10(c) and (d)).
(2) At each grid point the rank of the SSD composite with respect to the 300 random composites was estimated.
(3) A 99% confidence level is achieved if the SSD composite is ranked higher (or lower) than 297 (or 3) (see Moore *et al.* for more details).

Figure 10(a) shows Eulerian composites of 925 hPa geopotential height and vector wind. Dominant features are the marked eastward extension of the Azores high into the central Mediterranean Sea and a band of lower geopotential height along the southern side of the Saharan mountains/Sahel region. The pressure gradient between these areas generates strong northeasterly to northerly Etesian winds over Libya, Egypt and the northern parts of Chad and Sudan. There are some indications for blocking of this flow at the Aïr–Hoggar–Tibesti mountain chain and the Darfur Mountains, which could explain the marked low-pressure zone. There is, however, also some enhanced flow through the gaps between the Tibesti and the Ennedi on one side and the Hoggar on the other side. This points towards an important role of Saharan orography and an intensified trade wind regime for creating SSD disturbances. The northerly flow towards the Atlas Mountains might be an indication for blocking and lee cyclogenesis during the northwest African part of the track.

Anomalies with respect to 20-year (1989–2008) monthly means (Figure 10(b)) emphasise some of the characteristics discussed above. The eastward extension of the Azores high into the central Mediterranean Sea is associated with a weakly positive geopotential height anomaly of up to 2 gpm with an anticyclonic wind field. The Azores high itself is weaker than normal, pointing to the presence of North Atlantic troughs that may support cyclogenesis to the south of the Atlas as in the case-study discussed in section 3. A negative geopotential height anomaly is evident to the northwest of

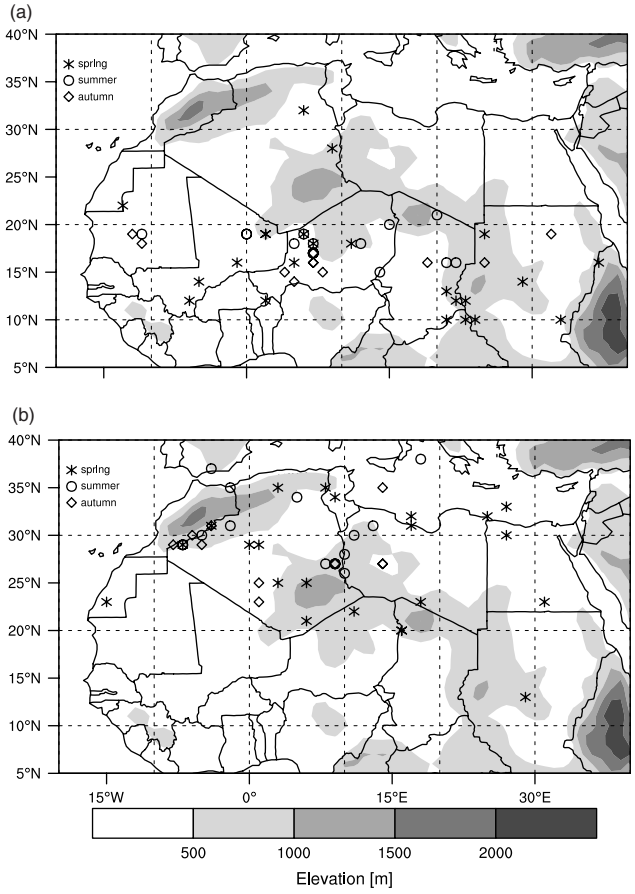

Figure 9. (a) Genesis and (b) lysis locations of the 50 SSDs identified during 1989–2008. Different symbols represent the seasons: spring (star), summer (circle) and autumn (diamond). No SSDs are identified for winter. Elevation (m) from the ERA-Interim model is given in shades of grey as in Figure 1.

the Hoggar Massif, related to a northward extension of the SHL during SSD situations.

Considering the first days of the 50 SSD tracks, i.e. the genesis, only results in a composite almost identical to Figure 10(a), but with a somewhat lower geopotential height over the central Sahara (Figure 10(c)). Large parts of this pattern are significant at a confidence level of 99% when compared to the background climatology. The analogous analysis for SSD lysis differs from the genesis composite through a somewhat weaker ridge over the western and central Mediterranean Sea and a northward extension of the trough over the central and west Sahara towards the Atlas Mountains (Figure 10(d)). The evolution of these two features during the SSD lifetime resembles a transition from the west to the east phase of Chauvin *et al.* (2010), despite the fact that changes in geopotential height over the Atlantic are weak. The relatively small difference between the genesis and lysis composites suggests that there is no coherent geopotential height evolution for SSDs. Looking at individual cases, several types of propagation can be identified. During most SSD cases, a ridge from the Atlantic or western Mediterranean Sea propagates eastward to the Gulf of Sidra, where it becomes stationary and often degrades under the influence of a pronounced heat low over the Arabian Peninsula and the Middle East. Frequently it re-strengthens due to a second ridge entering into the western Mediterranean Sea and migrating eastwards to the position of the first ridge. Sometimes this ridge then continues propagating eastwards toward the Middle East. In this way, genesis and lysis can look very similar over the Mediterranean despite the fact that the ridges propagate in the meantime. A second, less frequent type is characterised by only one ridge entering the Mediterranean Sea and propagating eastwards towards the Middle East. It is conceivable that the SSD propagation is also in some cases influenced by upper- or mid-level disturbances such as waves at the Subtropical Jet or non-AEW disturbances along the African Easterly Jet.

An Eulerian composite of OLR (Figure 11(a)) shows high values (rare occurrence of cold clouds) over the Sahara Desert and a decrease towards the Mediterranean and the Sahel–Soudan zone. Anomalies with respect to long-term monthly means (1974–1995) indicate positive anomalies of up to 6 W m^{-2} and thus reduced cloudiness over the central Saharan mountains, the Atlas Mountains and most parts of western Africa (Figure 11(b)). Negative OLR anomalies (up to -4 W m^{-2}) occur over the Great Western and Great Eastern Erg to the north of the Hoggar Massif. This is most likely the result of increased cloud cover and reduced surface air temperatures due to the advection of moist air from the Mediterranean Sea and SSD transitions into Mediterranean cyclones fostered by Atlas lee cyclogenesis. Over the rest of the domain the identified systems are not able to generate significant cloudiness. This result is consistent with insignificant rainfall anomalies associated with SSD situations (Figure 11(c) and (d)).

A TOMS AI composite indicates two regions with high aerosol concentrations (Figure 11(e)): West Africa centred over central Mali, and the Bodélé Depression as documented in numerous other studies. The Mali maximum coincides with a convergence zone (Figure 10(a)), where the northeasterly harmattan flow converges with the southerly monsoon winds. Convergence fosters accumulation of dust, a deep boundary layer and upward transport of dust. SSD-related anomalies are generally weak (-0.6 to 0.4) with positive values (enhanced aerosol concentration) over the central and eastern Sahara and negative values (decreased aerosol concentrations) over the western Sahara and the Atlas Mountains region (Figure 11(f)). The former might be due to the increased harmattan winds at the beginning of SSD episodes as documented in the case-study in section 3. The latter may be due to wind flow from the Atlantic advecting pristine maritime air into the desert (Figure 10(a) and (b)). No clear relation between SSD occurrence and increased aerosol concentration can be drawn. Overall these composite results largely contradict the literature, where SSDs have been reported to be associated with clouds, precipitation and dust.

Lagrangian composites of the same variables do not show significant signals in cloudiness, precipitation and dustiness either (not shown). Not even a clear cyclonic circulation is evident from wind composites. These results underline very clearly that the systems objectively identified and tracked do not fit the classical picture of SSDs as described in the literature, calling for a revision of the conceptual model as discussed in the following section.

6. Discussion

The characteristics of the weather systems described in the previous section do not agree well with the classical concept of SSDs summarized in the Introduction of this article. Significant differences are found during the initiation and

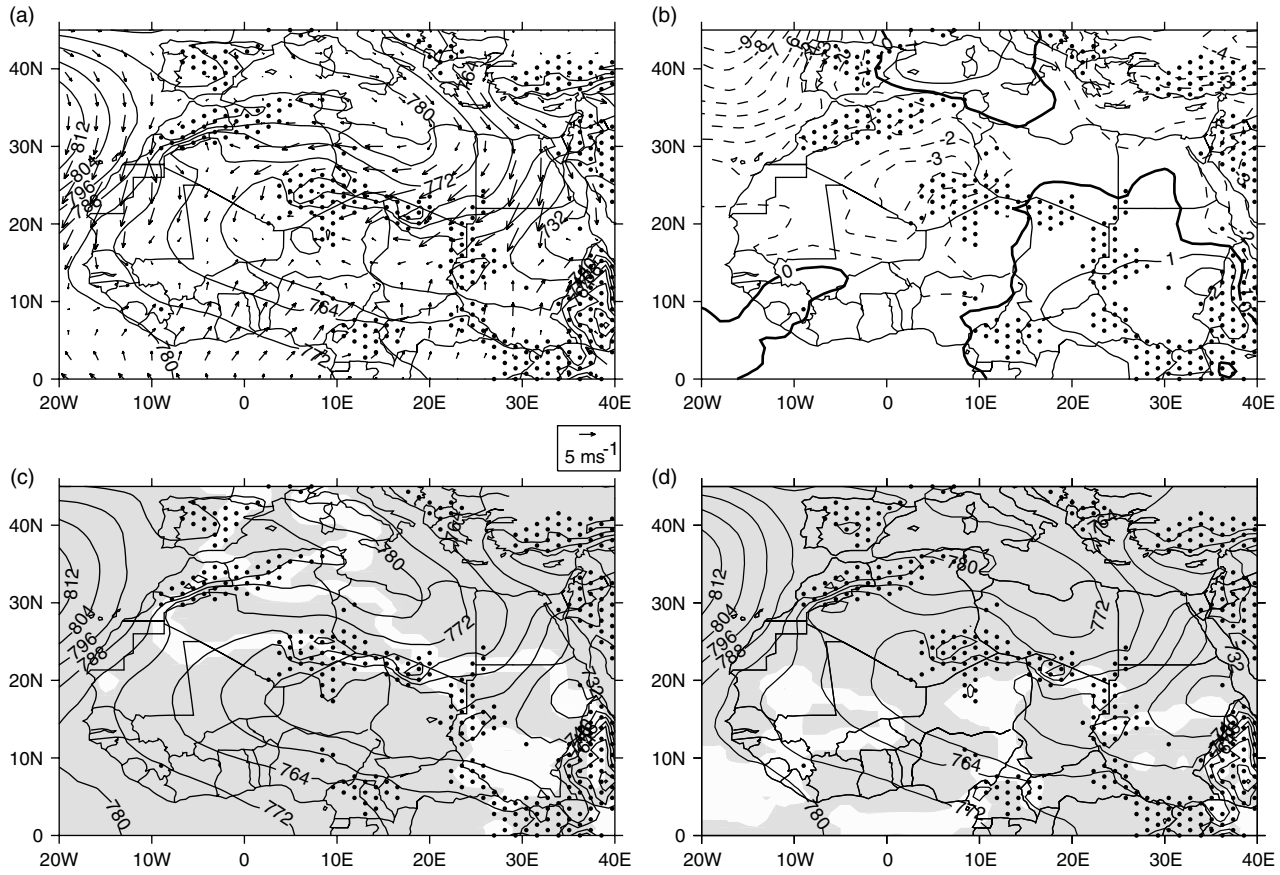

Figure 10. (a) Absolute and (b) anomaly composites of geopotential height and wind for all days with an identified SSD. (c) and (d) show geopotential height composites for the first and last dates of all identified SSD systems. Shaded areas indicate significance according to a confidence level of 99% (see beginning of section 5 for more details). Dotted areas indicate orography higher than 600 m as in Figure 1.

tracking phase, with respect to frequency of occurrence and seasonality, and with regard to accompanying rainfall and dust-storms.

In the following, two potential explanations for these differences will be discussed.

(A) Are the algorithm and/or the data used here not adequate for the problem? The authors acknowledge that objective identification and tracking algorithms generally suffer from a certain degree of arbitrariness when it comes to setting thresholds. In single cases, track splitting or merging can lead to ambiguities that are sometimes difficult to capture. However, the routine used here has been carefully adapted to the special circumstances over West Africa as detailed in section 2 and extensively tested through threshold variations and comparisons with subjective identification and tracking. In addition, the input data was varied using absolute values and anomalies, daily and 6-hourly data and different vertical levels (see section 2.3). The criteria to filter SSD-like disturbances out of all identified tracks are clearly based on the main characteristics described in the literature and are rather relaxed (northward track starting to the south of 20°N and covering at least 10 degrees latitude over a broad North African region). The authors therefore doubt that a differently designed algorithm would be able to identify substantially more SSD-like disturbances. Another source of error is, of course, the input data themselves. Re-analyses generally require synoptic data as observational constraints, which are sparse over the Sahara Desert compared to many other regions, enhancing the weight of the numerical model used in the analysis procedure. Given that the ERA-Interim data used here were generated with a 4D-Var assimilation system, a considerable amount of non-synoptic information was included. Overall, the authors expect this dataset to be of sufficient quality to realistically represent synoptic-scale features such as SSDs, even in a data-sparse region such as the Sahara.

(B) Is the classical conceptual model inaccurate? As stated in the Introduction, SSDs were first described in the 1930s based on a very coarse network of surface stations. It is conceivable that this led to a misinterpretation of the available observations. Many studies have described cases of unsettled weather in the Sahara associated with rainfall and dust-storms. These two phenomena are often connected through the evaporation of precipitation leading to haboobs. Such situations can be caused by unusually strong AEWs with a pronounced southerly sector bringing moisture much further north than usual (Cuesta *et al.*, 2010) and/or troughs penetrating equatorward at upper levels that destabilize the atmosphere and create uplift. These two effects can also interact as suggested by Nicholson (1981) and described by Knippertz *et al.* (2009), Lavaysse *et al.* (2009) and Knippertz and Todd (2010) among others. If the moisture source is in the Soudan zone, the unsettled weather spreads northward into the Sahara and, at later stages, moisture from the Mediterranean Sea can contribute to rainfall associated with the subtropical upper-level trough. The early descriptions of SSDs might well have associated such a succession of events with a moving depression in the surface pressure field as commonly observed at midlatitudes. This study has for the first time provided evidence that this is often not

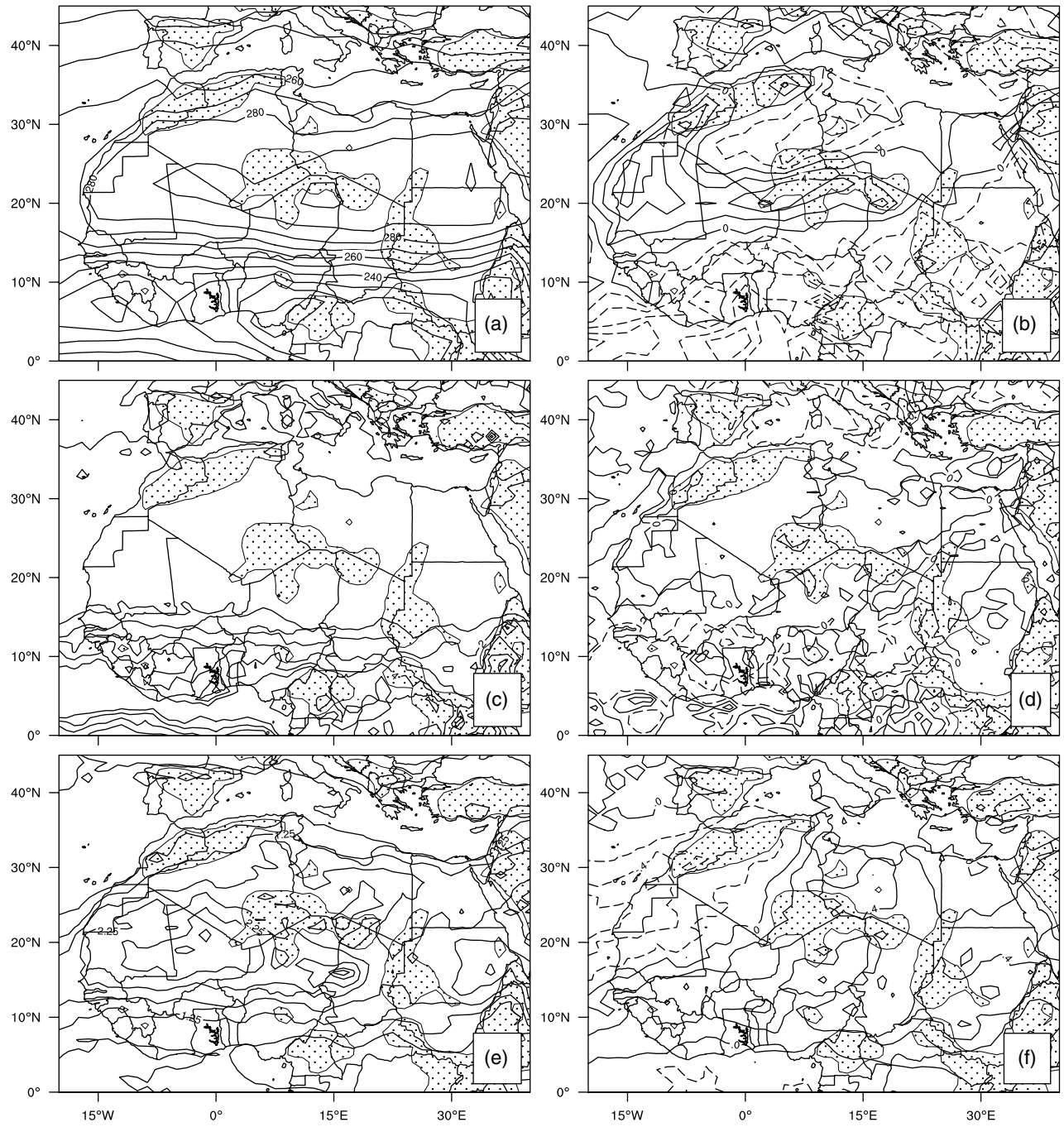

Figure 11. Absolute (left panels) and anomaly (right panels) composites for all days with an identified SSD. (a) and (b) NOAA outgoing long-wave radiation (OLR) (W m^{-2}), (c) and (d) TRMM 3B42 daily precipitation (mm d^{-1}), and (e) and (f) TOMS UV Aerosol Index (unitless). Dotted areas indicate orography higher than 600 m as in Figure 1.

the case. Potential reasons that oppose this are the strong contributions from sensible heat fluxes and evaporative cooling together with orographic influences. Consequently, 'Soudano-Saharan Depression' does not appear an adequate term for this kind of situation and should not be used in the way it has been in various textbooks. The more general 'Soudano-Saharan Disturbance' or simply 'Saharan Disturbance' are much more adequate terms in our eyes. It is unclear, however, what criteria are best suited to objectively identify these situations to test whether the seasonality and other characteristics assigned to SSDs are fulfilled. Precipitation and/or dustiness are probably the best candidates, but such an investigation is beyond the scope of this study.

7. Conclusions

Since the 1930s, SSDs have been described in the literature as surface depressions that form over the Sahel/Soudan zone, initially track westward and then turn anticyclonically into the Sahara and sometimes even into the Mediterranean Sea (Dubief and Queney, 1935; Dubief, 1947). SSDs have been linked with precipitation and dust-storms. For the first time this study verified this concept using an objective identification and tracking algorithm together with modern re-analysis and satellite data. Despite a careful design of the employed tools, only 50 depressions were identified in 20 years of ERA-Interim re-analysis data. Unexpectedly, these systems do not follow the seasonally varying tracks

described in the literature and show limited relevance for cloudiness, rainfall and dust-storms.

Instead, the formation of the identified systems appears to be closely related to orographic blocking effects of cold air surges from the Mediterranean by the central Saharan mountain ranges (Tibesti, Hoggar, Adrar des Iforas, Aïr). No coherent mechanism for the westward propagation of the systems could be identified, with only less than a third of the identified cases showing a relation to AEWs, in contrast to the literature (Nicholson, 1981).

The results of this study strongly suggest that the classical SSD concept is a misinterpretation of the limited (and mainly surface-based) observations available to the meteorologists who first described this phenomenon. The unsettled weather in the Sahara (rain and dust-storms) typically associated with SSDs are in fact often related to interactions of AEWs and subtropical upper-level waves (e.g. Knippertz *et al.*, 2009; Knippertz and Todd, 2010), but these situations do not generally generate trackable surface depressions. The authors therefore suggest calling this phenomenon a 'Saharan Disturbance' and substantially revising the respective sections in various textbooks. Future studies should try to find a clear, scientifically sound definition for the described weather events, which will most likely have to concentrate on mid- and upper-levels of the troposphere rather than the surface.

Acknowledgements

This work was funded by the DFG (German Research Foundation) Emmy Noether programme (grant KN 581/3-2). Many thanks to Andreas Fink for discussion and to Heini Wernli for providing and explaining the identification algorithm. The authors also thank Andreas Macke and the IFM-GEOMAR, Kiel, Germany for providing MSG data. Interpolated OLR data are provided by the NOAA/OAR/ESRL PSD, Boulder, Colorado, USA, through their Web site at http://www.esrl.noaa.gov/psd/and TRMM 3B42 data by the NASA/Goddard Space Flight Center's Laboratory for Atmospheres and TSDIS, which develop and compute the product as a contribution to TRMM. Thanks to the TOMS mission scientists and associated NASA personnel for the production of the data used in this study. The authors thank the ECMWF for providing ERA-Interim re-analysis data, and two anonymous reviewers for their helpful comments.

References

Alpert P, Ziv B. 1989. The Sharav Cyclone: Observations and some theoretical considerations. *J. Geophys. Res.* **94**: 18495–18514.

Barnston AG, Livezey RE. 1987. Classification, seasonality and persistence of low-frequency atmospheric circulation patterns. *Mon. Weather Rev.* **115**: 1083–1126.

Berrisford P, Dee D, Fielding K, Fuentes M, Kållberg P, Kobayashi S, Uppala S. 2009. '*The ERA-Interim archive*.' ERA Report Series 1. ECMWF: Shinfield Park, Reading.

Buckle C. 1996. *Weather and Climate in Africa*. Longman.

Chauvin F, Roehrig R, Lafore J-P. 2010. Intraseasonal variability of the Saharan Heat Low and its link with midlatitudes. *J. Climate* **23**: 2544–2561.

Couvreux F, Guichard F, Bock O, Lafore J-P, Redelsperger J-L. 2010. Synoptic variability of the monsoon flux over West Africa prior to the onset. *Q. J. R. Meteorol. Soc.* **136**(S1): 159–173.

Cuesta J, Lavaysse C, Flamant C, Mimouni M, Knippertz P. 2010. Northward bursts of the West African monsoon leading to rainfall over the Hoggar Massif, Algeria. *Q. J. R. Meteorol. Soc.* **136**(S1): 174–189.

Drobinski P, Sultan B, Janicot S. 2005. Role of the Hoggar massif in the West African monsoon onset. *Geophys. Res. Lett.* **32**: L01705, DOI: 10.1029/2004GL020710.

Dubief J. 1947. Les pluies au Sahara central. *Trav. Inst. Rech. Sahariennes* **IV**: 7–23.

Dubief J. 1963. *Le Climat du Sahara*. Mémoires I.R.S.: Algier.

Dubief J, Queney P. 1935. Les grands traits du climat du Sahara algérien. *La Météorologie* **XI**: 80–91.

Egger J, Alpert P, Tafferner A, Ziv B. 1995. Numerical experiments on the genesis of Sharav cyclones: Idealized simulations. *Tellus* **47A**: 162–174.

Fink AH, Reiner A. 2003. Spatiotemporal variability of the relation between African Easterly Waves and West African squall lines in 1998 and 1999. *J. Geophys. Res.* **108**: 4332, DOI: 10.1029/2002JD002816.

Flohn H. 1975. Tropische Zirkulationsformen im Lichte der Satellitenaufnahmen. P 82 in *Bonner Meteorologische Abhandlungen, Sonderheft*. Westdeutscher Verlag: Opladen.

Griffiths JF, Soliman KH. 1972. The northern desert (Sahara). Chapter 3, pp 75–132 in *World Survey of Climatology, Climates of Africa, Vol. 10.* Elsevier.

Herman JR, Bhartia PK, Torres O, Hsu C, Seftor C, Celarier E. 1997. Global distribution of UV-absorbing aerosols from Nimbus 7/TOMS data. *J. Geophys. Res.* **102**: 16911–16922.

Horvath K, Fita L, Romero R, Ivančan-Picek B. 2006. A numerical study of the first phase of a deep Mediterranean cyclone: Cyclogenesis in the lee of the Atlas Mountains. *Meteorol. Z.* **15**: 133–146.

Howell FC, Bourlière F (eds). 1963. *African Ecology and Human Evolution*. Routledge: London.

Huffman GJ, Adler RF, Bolvin DT, Gu G, Nelkin EJ, Bowman KP, Hong Y, Stocker EF, Wolff DB. 2007. The TRMM Multisatellite Precipitation Analysis (TMPA): Quasi-global, multiyear, combined-sensor precipitation estimates at fine scales. *J. Hydrometeorol.* **8**: 38–55.

Hurrell JW. 1995. Decadal trends in the North Atlantic Oscillation: Regional temperatures and precipitation. *Science* **269**: 676–679.

Issar AS. 1995. '*Impacts of climate variations on water management and related socio-economic systems*.' Technical Documents in Hydrology, IHP-UNESCO. Paris. Sc.95/Ws.26, 97 pp.

Jones PD, Jonsson T, Wheeler D. 1997. Extension to the North Atlantic Oscillation using early instrumental pressure observations from Gibraltar and south-west Iceland. *Int. J. Climatol.* **17**: 1433–1450.

Knippertz P, Todd MC. 2010. The central west Saharan dust hot spot and its relation to African easterly waves and extratropical disturbances. *J. Geophys. Res.* **115**: D12117, DOI: 10.1029/2009JD012819.

Knippertz P, Ansmann A, Althausen D, Müller D, Tesche M, Bierwirth E, Dinter T, Müller T, von Hoyningen-Huene W, Schepanski K, Wendisch M, Heinold B, Kandler K, Petzold A, Schütz L, Tegen I. 2009. Dust mobilization and transport in the northern Sahara during SAMUM 2006 – A meteorological overview. *Tellus* **61B**: 12–31.

Lavaysse C, Flamant C, Janicot S, Parker DJ, Lafore J-P, Sultan B, Pelon J. 2009. Seasonal evolution of the West African heat low: A climatological perspective. *Clim. Dyn.* **33**: 313–330.

Lavayasse C, Flamant C, Janicot S, Knippertz P. 2010. Links between African easterly waves, midlatitude circulation and intraseasonal pulsations of the West African heat low. *Q. J. R. Meteorol. Soc.* **136**(S1): 141–158.

Leroux M. 2001. *The Meteorology and Climate of Tropical Africa*. Springer.

Liebmann B, Smith CA. 1996. Description of a complete (interpolated) outgoing longwave radiation dataset. *Bull. Am. Meteorol. Soc.* **77**: 1275–1277.

Moore RW, Martius O, Davies HC. 2008. Downstream development and Kona low genesis. *Geophys. Res. Lett.* **35**: L20814, DOI: 10.1029/2008GL035502.

Nicholson SE. 1981. Rainfall and atmospheric circulation during drought periods and wetter years in West Africa. *Mon. Weather Rev.* **109**: 2191–2208.

Nicholson SE. 2000. The nature of rainfall variability over Africa on times scales of decades to millennia. *Global and Planetary Change* **26**: 137–158.

Nicholson SE, Flohn H. 1980. African environmental and climatic changes and the general atmospheric circulation in late Pleistocene and Holocene. *Clim. Change* **2**: 314–348.

Pedgley DE. 1972. Desert depression over north-east Africa. *Meteorol. Mag.* **101**: 228–244.

Schepanski K, Tegen I, Laurent B, Heinold B, Macke A. 2007. A new Saharan dust source activation frequency map derived from MSG-SEVIRI IR-channels. *Geophys. Res. Lett.* **34**: L18803, DOI: 10.1029/2007GL030168.

Schepanski K, Tegen I, Todd MC, Heinold B, Bönisch G, Laurent B, Macke A. 2009. Meteorological processes forcing Saharan dust emission inferred from MSG-SEVIRI observations of subdaily dust

source activation and numerical models. *J. Geophys. Res.* **114**: D10201, DOI: 10.1029/2008JD010325.
Sultan B, Janicot S. 2003. The West African monsoon dynamics. Part II: The 'preonset' and 'onset' of the summer monsoon. *J. Climate* **16**: 3407–3427.
Thorncroft CD, Flocas HA. 1997. A case study of Saharan cyclogenesis. *Mon. Weather Rev.* **125**: 1147–1165.
Vizy EK, Cook KH. 2009. A mechanism for African monsoon breaks: Mediterranean cold air surges. *J. Geophys. Res.* **114**: D01104, DOI: 10.1029/2008JD010654.
Warner TT. 2004. *Desert Meteorology*. Cambridge University Press.
Wernli H, Schwierz C. 2006. Surface cyclones in the ERA-40 dataset (1958–2001). Part I: Novel identification method and global climatology. *J. Atmos. Sci.* **63**: 2486–2507.

